Appl. Phys. B (2017) 123:141
DOI 10.1007/s00340-017-6717-8

Applied Physics B
Lasers and Optics

Off-beam quartz-enhanced photoacoustic spectroscopy-based sensor for hydrogen sulfide trace gas detection using a mode-hop-free external cavity quantum cascade laser

Marek Helman[1] · Harald Moser[2] · Alina Dudkowiak[1] · Bernhard Lendl[2]

Received: 30 November 2016 / Accepted: 30 March 2017 / Published online: 13 April 2017

Abstract Hydrogen sulfide (H_2S) trace gas detection based on off-beam quartz-enhanced photoacoustic spectroscopy using a continuous wave (CW), mode-hop-free external cavity (EC) quantum cascade laser tunable from 1310 to 1210 cm^{-1} was performed. A 1σ minimum detection limit of 492 parts per billion by volume (ppbv) using a 1 s lock-in time constant was obtained by targeting the line centered at 1234.58 cm^{-1}. This value corresponds to a normalized noise equivalent absorption coefficient for H_2S of 3.05×10^{-9} W cm^{-1} $Hz^{-1/2}$.

1 Introduction

The sensitive and selective detection of gaseous sulfur species with the emphasis on hydrogen sulfide (H_2S) down to trace concentrations is of essential importance across a wide range of applications including production control and environmental monitoring purposes in the field of petrochemical, paper, and pulp or biotechnological processes. The wide occurrence of H_2S in these processes, and due to its negative impact on process stability and product quality, the concentration of H_2S needs to be tightly monitored [1]. Furthermore, personal safety considerations and legal concentration limits also necessitate the accurate determination of H_2S levels. The occupational exposure limit recommended by the European Agency for Safety and Health at Work (EU-OSHA) is 5 ppmv [2]. The permissible exposure limit value for H_2S is 10 ppmv, the Immediately Dangerous to Life and Health (IDLH) level is 300 ppmv and lethal concentrations are in the range of 2000 ppmv [2]. In practice, concentrations ranging from sub-ppmv levels at low pressures to several per cents at atmospheric conditions need to be monitored. Despite a variety of online monitoring options for gaseous H_2S, its reliable quantitative and selective determination still remains challenging in the field of chemical sensors [3–5].

In the field of laser spectroscopy, the constant improvement of quantum cascade lasers (QCLs) has led to their application as reliable sources of coherent light ranging from the mid-infrared (MIR) to the terahertz spectral region for sensitive detection of molecular species on their fundamental vibrational, respectively, rotational bands [6–9]. Due to their tailorable emission wavelength, high output power, compactness, narrow spectral linewidth, and wavelength tuneability, QCLs are optimal choices for spectroscopic applications. In addition, optical resonator designs are constantly improved over the years with the distributed feedback (DFB) [10] and the external cavity (EC) [11] approach being the most prominent ones. A general aim with respect to the ongoing development of QCLs for sensing applications is to reduce the line width of the emitted radiation to a minimum while achieving a spectral coverage as large as possible. So far, EC-QCLs offer the largest tuning range which, depending on the employed gain medium, may cover up to several hundreds of wavenumbers. The external cavity design facilitates broadband spectral tuning by an external diffraction grating, while the selection of the emission wavelength takes place by changing the grating angle relative to the QCL chip.

✉ Alina Dudkowiak
alina.dudkowiak@put.poznan.pl

[1] Faculty of Technical Physics, Poznan University of Technology, Piotrowo 3, 60-965 Poznan, Poland

[2] Institute of Chemical Technologies and Analytics, Vienna University of Technology, Getreidemarkt 9/164, 1060 Vienna, Austria

Technically viable setups for H_2S trace gas measurements in the MIR spectral region using QCLs are often chosen to be based on absorbance measurements in multi-reflection Herriott cells [12] as the effective optical interaction pathlength will be increased up to several tens of meters. Recently, the first application of ring-cavity-surface-emitting quantum-cascade lasers (RCSE-QCLs) for sensitive H_2S gas measurements was reported [13]. Together with phase-sensitive detection techniques, such as wavelength modulation spectroscopy (WMS) [14, 15], the generally dominating $1/f$ electronic noise can be drastically minimized, and in general, high detection sensitivities of H_2S can be achieved, enabling on-line monitoring of H_2S and CH_4 content in a petrochemical process stream [16]. Complementary to the direct absorption approach, photoacoustic spectroscopy (PAS) detects pressure waves which are caused by a thermal expansion of the gas due to non-radiative relaxation of molecules after absorption of modulated laser radiation. Conventional PAS utilizes broadband condenser or electret microphones as acoustic transducer [17]. A variant of the classical approach, called quartz-enhanced photoacoustic spectroscopy (QEPAS), employs a quartz tuning fork (QTF) as a sharply resonant acoustic transducer to detect weak photoacoustic excitations [18]. The QTF is an mm-sized piezoelectric element, which converts a deformation caused by acoustic waves into charges that can be measured by its electrodes. Commercial readily available QTFs, which are designed as frequency standard for smartphones, watches, and clocks, are low-cost oscillators with a resonance frequency of 32,768 Hz and a quality that can exceed 100,000 in vacuum [19]. Only the anti-symmetric QTF vibration, i.e., when the two prongs bend in opposite directions, is piezo-electric active [20]. Thus, in a typical QEPAS arrangement, the laser beam is transmitted through the gap of the QTF formed by the two tines to probe strong photoacoustic signals. A significant enhancement of the detected QEPAS signal can be achieved when an acoustic resonator is added to the QTF. In case of the typical on beam configuration, a tube is added in front and behind the QTF, exploiting a longitudinal acoustic resonance [20]. By this means, a 30-fold increase in the SNR compared to the bare tuning fork can be achieved [21]. In principal, the noise of a QEPAS sensor is determined by the thermal noise of the QTF. However, additional noise can be introduced by unintended illumination of the transducer. The gap formed by the two tines is only 300 μm, which makes it often difficult to focus the beam through this configuration. An alternative resonator focuses the excitation beam with some lateral displacement in parallel to the two QTF tines through an acoustic resonator consisting of only a single tube [22]. This configuration is referred to as off-beam QEPAS. The resonator has a small aperture in the middle to enable generated pressure waves to exit and to couple with the QTF, which is positioned closely to the aperture. The benefit of this off-beam configuration is that the laser beam has not to be focused through the narrow gap of the QTF and yields a 17-fold improvement in the SNR. A refined version of the singe tube off beam resonator has been shown by a T-shape resonator consisting of a main pipe and a short branch pipe [23], exhibiting comparable improvements in sensitivity as the on-beam configuration. A slightly different way of protecting the QTF from unwanted scattered irradiation based on the use of two acoustically coupled micro-resonators was also presented [24].

Recent QEPAS sensors have been designed mostly as field operations ready. Successful application for atmospheric CH_4 and N_2O measurements near Greater Huston area landfills using QCL-based QEPAS sensor was reported in 2014 [25].

Different QEPAS setups monitoring H_2S have been demonstrated. In the 2.6 μm region, the detection limit of 500 part per billion by volume (ppbv) for 1-min integration [26], and in mid-IR region, 330 ppbv for integration time of 30 s have been achieved [27]. A THz QEPAS H_2S sensor with detection sensitivity of 7 ppmv for a 4-s averaging time has also been demonstrated [28–30].

This paper reports on the design and realization of a mid-IR off-beam QEPAS sensor utilizing an MHF EC-QCL as the spectroscopic light source for the selective and sensitive detection of H_2S traces.

To the best of the authors knowledge, this is the first paper in which the selected H_2S line at 1234.56 cm^{-1} is targeted for concentration measurements in the QEPAS sensors. By employing the off-beam configuration to deal with EC-QCL beam irradiating the QTF during absorption profile scan, we were able to manage higher than 1-s integration time sensitivity than in the previously reported QEPAS systems designed for H_2S detection [26, 27, 30–32].

2 Experimental setup

2.1 CW MHF EC-QCL characterization

A water-cooled continuous wave mode-hop-free external cavity quantum cascade laser (CW MHF EC-QCL) (*41078-MHF, Daylight Solutions, CA, USA*) emitting at a center wavelength of $\lambda = 7.9$ μm was employed as an efficient and widely tunable spectroscopic source generating up to 180 mW of optical power. The EC-QCL was coarsely tunable over 90 cm^{-1} in the stepping motor grating tuned operation mode in the range from 1310 to 1220 cm^{-1}. Here, the angular position of the internal EC grating is controlled via

the built-in stepping motor with a minimum step width of 0.01 cm^{-1}. For fine wavelength tuning or coarse modulation of up to 1.0 cm^{-1} at a maximum frequency of 60 Hz, once the center wavelength has been set, and an externally driven (unipolar 0–100 V) PZT is installed in the drive train to mechanically modulate the grating. Higher modulation frequencies can be accomplished via direct current modulation in the frequency range between 10 kHz and 2 MHz by applying up to a 4.5 V_{pp} sine wave to the input on the laser head leading to a maximum wavelength modulation depth of up to 0.1 cm^{-1}. Since the laser can be modulated at various places on the gain curve, the depth of amplitude modulation (AM) will change for different wavelengths. It should be noted that both modulation/fine tuning methods can be used separately as well as simultaneously. The combined approach is used for wavelength modulation spectroscopy (WMS).

The mode-hop-free operation and the time-resolved spectral tuning behavior of the EC-QCL in the 1236–1234 cm^{-1} spectral range were investigated using a Fourier-Transform IR spectrometer with a stepscan attachment (Bruker Vertex 80v, Bruker Optics, Germany) with 0.075 cm^{-1} spectral and 2-ns temporal resolution [33, 34]. An exemplary time-resolved spectrum for 50-Hz sinusoidal PZT voltage ramp (at 400-mA laser current and 18.5 °C laser temperature) ranging from 0 to 100 V recorded in combination with an 8-bit resolution and 500-MS/s sample rate transient recorder board (Spectrum GmbH, Germany) is shown in Fig. 1a. Figure 2b shows that the depth of laser tuning is 1.0 cm^{-1}, and because of the nature of EC, a strong intensity modulation of the light emitted is observed (Fig. 1c).

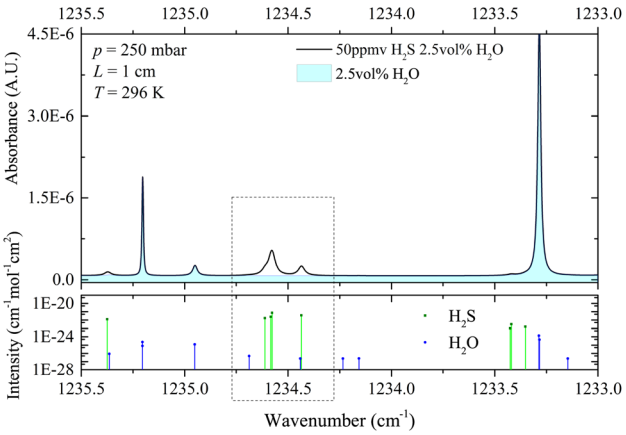

Fig. 2 HITRAN2012 simulated absorbance spectrum of 50 ppmv H_2S together with 2.5% H_2O (*blue shaded area*) in N_2 in the PZT tuning range of the EC-QCL. The sample pressure is set to 250 mbar, the absorption path to 1 cm, and the temperature to 296 K

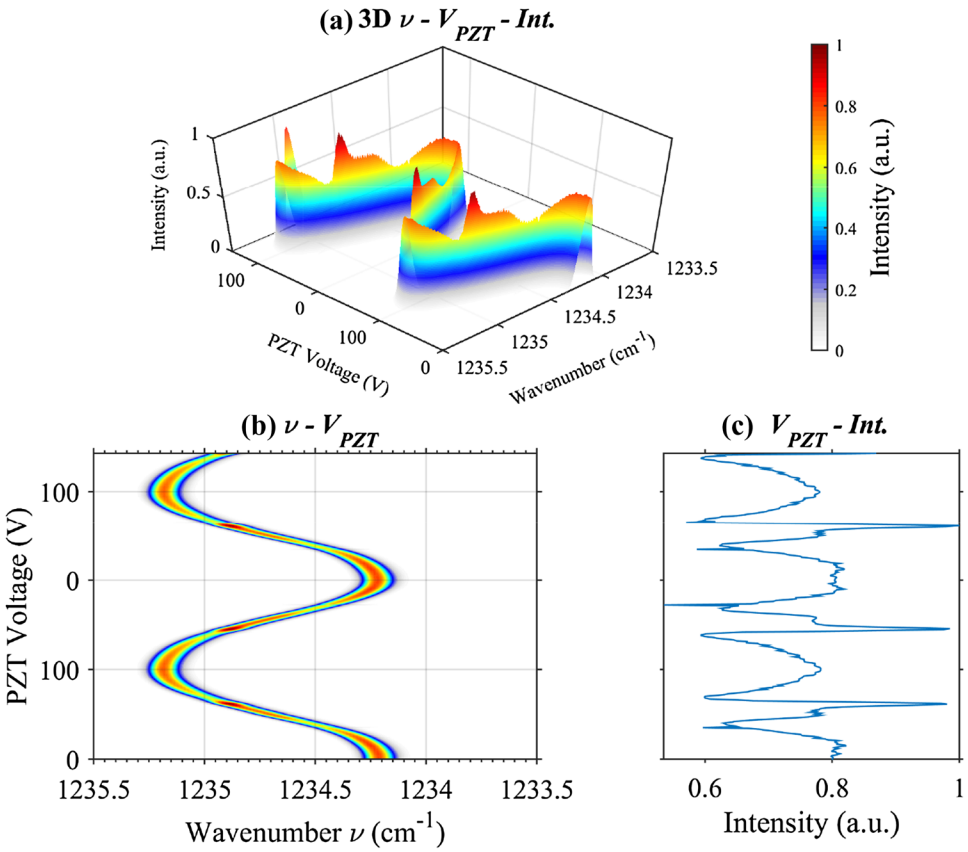

Fig. 1 **a** Spectrally and time-resolved tuning behavior of the EC-QCL centered around 1234.6 cm^{-1} during a sinusoidal PZT scan in the range of 0–100 V is shown by the *top* and *side* views of this graph, respectively, **b** tuning range, and **c** intensity modulation of the EC-QCL. The laser current is set to 400 mA and laser temperature is 18.5 °C

2.2 H_2S line selection

To perform selective H_2S QEPAS measurements, the absorption lines centered around 1234.58 cm^{-1} of the ν_2 -bending-mode transition of H_2S were chosen. Although the sensor investigation in this work was limited to certified H_2S in N_2 mixtures, the possibility of water (H_2O) interference is investigated via simulation. With regard to the possible presence and influence of H_2O, reference spectra of 50 ppmv H_2S along with 2.5 vol% H_2O at a pressure of 250 mbar and 1 cm optical path length were calculated based on the HITRAN2012 [35] database (Fig. 2). Negligible spectral interference can be expected from H_2O lines in this wavenumber region. Moreover, since H_2S shows fast vibrational de-excitation, similar to that of H_2O [36], there is no relaxation promotion for a humidified gas mixture [27].

2.3 Sensor system architecture and operation principle

The T-shaped microresonator (mR)-based QEPAS spectrophone configuration [37] was used, to avoid additional noise introduced by unintended illumination of the QTF caused by slight variations of the pointing stability of the emitted beam during mechanical PZT grating operation, including any scattered light and incidental reflections from optical elements. As the gap between the QTF prongs is only ~300 μm wide and the manufacturer specified pointing stability of the EC-QCL system is ~1 mrad during PZT operation, the maximum distance of the laser source to the QTF should not exceed ~300 mm for an optimal focused beam to avoid unintended illumination.

The off-beam QEPAS sensor system architecture is depicted in Fig. 3. The EC-QCL beam was focused with a CaF_2 lens ($f = 40$ mm) into a compact QEPAS gas cell, which contained the QTF and T-shaped acoustic resonator of 5.5 mm in length and 0.8 mm in diameter, designed for off-beam (OB) configuration [37], a gas in- and outlet connectors, and two ZnSe windows (AR coated). The Q-factor of the QTF used in this work was 12986 at a pressure of 250 mbar, and the QTF resonant frequency $f_0 = 32755.23$ Hz.

The sensor platform was based on 2*f* wavelength modulation spectroscopy (2*f*-WMS) and QEPAS detection [38]. The 2*f*-WMS operation mode provides suppression of the acoustic background by nonselective absorbers. In this case, the noise level is primarily determined by the thermal noise of the QTF [39]. To implement the 2*f*-WMS technique, the emission wavelength of MHF EC-QCL was modulated at half of the QTF resonance frequency $f_{mod} = f_0/2$ by embedding a sinusoidal modulation with a maximum amplitude of 4.5 V_{pp} provided by the function generator superimposed on the EC-QCL current through an internal bias. The detection of the QTF

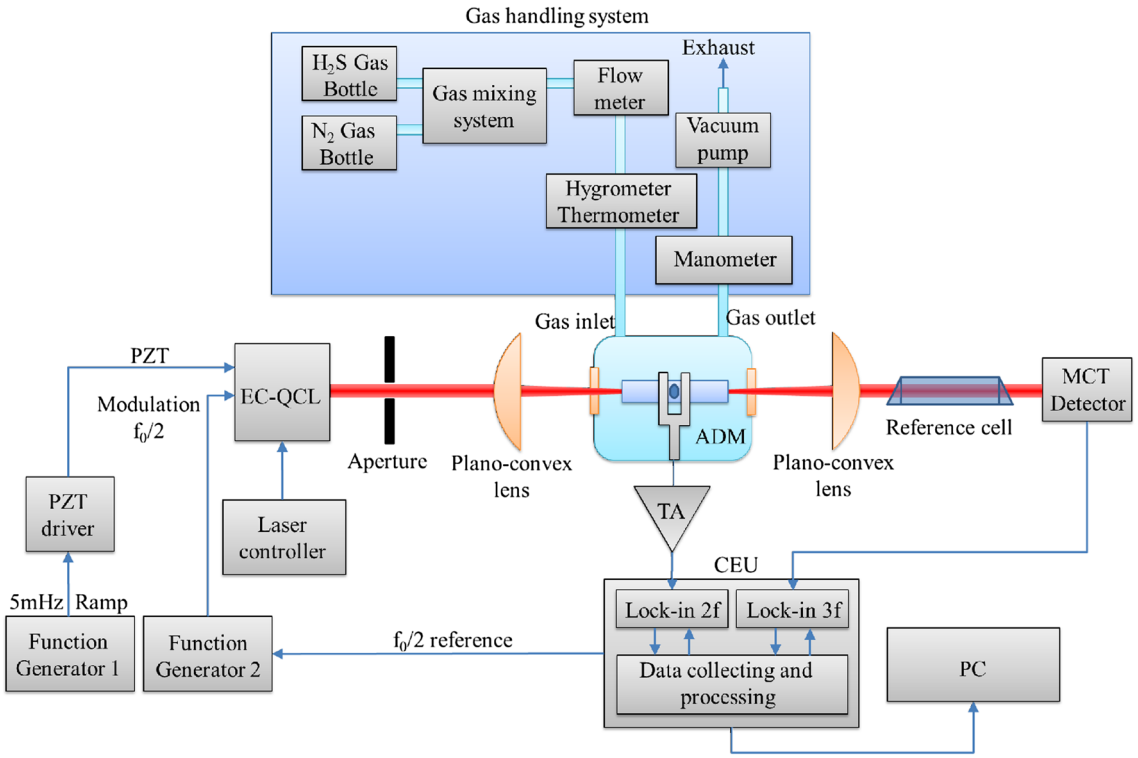

Fig. 3 Schematic diagram of the off-beam QEPAS-based H_2S sensor employing a CW MHF EC-QCL, where *TA* is transimpedance amplifier

signal was performed at f_0, using an internal lock-in amplifier with a time constant set to 1 s. A reference cell filled with a mixture of H_2S and N_2 gases (H_2S:N_2, 98:2%) at a pressure of 50 mbar and a mercury cadmium telluride (MCT) detector (PVI-2TE-10.6, Vigo Systems, Poland) located after the acoustic detection module (ADM) were used to monitor the 3*f* signal of the transmitted beam. The QEPAS detection was carried out in scan mode. A 5-mHz saw tooth waveform from the function generator was first amplified using a piezoelectric transducer (PZT) driver. The amplified signal of 24.2–43.2 V was then applied to the PZT element of the EC-QCL to mechanically modulate the external cavity grating. It allows a scan of the emitted frequency over the desired spectral range, to acquire spectral information of the gas sample.

Acoustic waves interacting with the QTF cause a vibration of its prongs and, therefore, generate a piezoelectric current in the element. The piezoelectric current was converted to a voltage signal by an ultra-low noise transimpedance amplifier with a 10-MΩ feedback resistor and was subsequently transferred to a QEPAS control electronics unit (CEU) (CDP Systems, Russian Federation). This unit allowed the measurement of QTF parameters and measurement of the 2*f* component of QTF, as well as the 3*f* component of the photodetector signal. Further data processing is carried out with a LabVIEW-based program by transferring the digitized data to a PC.

A high-resolution broadband pyroelectric array camera (Pyrocam III-HR, Ophir Optronics, Israel) was used to profile the laser beam transmitted through the QEPAS spectrophone for optical alignment verification. The optical power of the collimated laser beam was measured by a commercial power meter (Solo 2, Gentec-EO, Canada).

2.4 Sample preparation system

Different H_2S concentration levels within the range of 0–200 ppmv were achieved by dynamic dilution of a certified 1000 ppm H_2S:N_2 calibration gas with ultra-high purity N_2 using a custom-made gas mixing and conditioning system. Pressure and flow of the sample gas inside the ADM were controlled and maintained at the optimum constant level using a needle valve, manometer, pressure controller, and a vacuum pump. The flow rate of the dry gas mixture was kept constant at 25 ml min^{-1}.

3 Experimental results and discussion

3.1 Determination of optimum QEPAS operating parameters

The influence of the gas pressure and the WM amplitude on the QEPAS response was investigated to determine the optimal operating conditions in terms of off-beam QEPAS

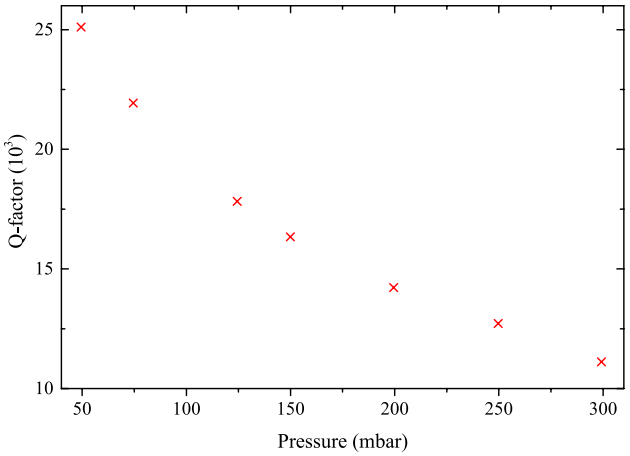

Fig. 4 Dependence of the Q-factor of QTF as a function of pressure

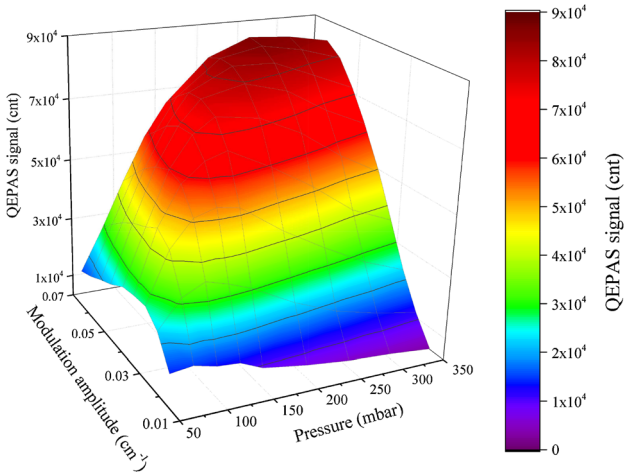

Fig. 5 Sensor optimization surface acquired at different operation pressures and modulation depths for a gas mixture of 200 ppmv H_2S in dry N_2

signal-to-noise ratio (SNR). At each pressure level (50–300 mbar), the QTF parameters f_0 and Q were measured (Fig. 4) and the laser modulation depth was varied in the range of 0.5 and 4.9 V_{pp}, which corresponded to a wavelength modulation depth between 0.015 and 0.070 cm^{-1}. Figure 5 shows the obtained results for a dry gas mixture composed of 200 ppmv H_2S in N_2. The optimal operating conditions for the sensor were found to be the gas pressure of 250 mbar and modulation amplitude $m_a = 0.065$ cm^{-1}.

3.2 Sensitivity and linear response of the off-beam QEPAS-based H_2S sensor system

For the selected H_2S absorption line centered at 1234.58 cm^{-1}, the optical power emitted by the MHF EC-QCL was ~160 mW. The laser beam was focused through the

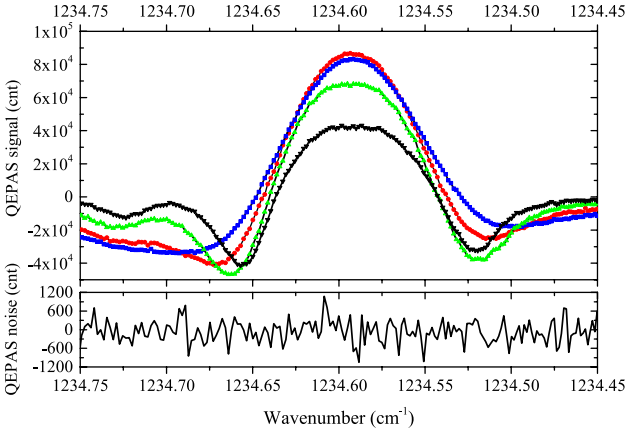

Fig. 6 Off-beam QEPAS signal of 2*f* WMS for 200 ppmv H_2S in dry N_2 when the laser was tuned across the absorption line located at 1234.58 cm^{-1} at the optimum working condition: $m_a = 0.065$ cm^{-1} and $p = 250$ mbar (*red line*), 350 mbar (*blue line*), 150 mbar (*green line*), and 100 mbar (*black line*)

resonator with a transmission efficiency of 99%. The optical power measured at the focal point was ~121 mW due to optical power losses by sensor system components, i.e., the aperture and CaF_2 lens. Considering the absorption of the ZnSe window and the transmission efficiency, the optical power of ~118 mW was directed through the resonator. The evaluation of the H_2S off-beam QEPAS sensor sensitivity was investigated for dry sample gas mixtures. The QTF signal was detected at f_0 and the optimum operating settings. Figure 6 shows the acquired 2*f* WMS signal for the dry gas mixture of 200 ppmv H_2S in N_2 and noise signal for N_2 at the flow rate of 25 ml min^{-1} for different pressures.

Off-beam QEPAS spectral scan acquisitions were obtained for different H_2S concentration levels within the range from 0 to 200 ppmv. Figure 7 shows the measured off-beam QEPAS amplitudes as a function of H_2S concentration. A linear fit of the data demonstrates good linearity of the sensor indications versus H_2S concentration ($R^2 = 0.99956$). The standard deviation (1σ) of the measured data points recorded by the ADM filled with N_2 was 246 counts. For a dry mixture of 30 ppmv H_2S in N_2, the determined QEPAS SNR was 61, which resulted in a minimum detection limit 492 ppbv. The time constant of the lock-in amplifier was set to 1 s, yielding an equivalent noise bandwidth of $\Delta f = 0.785$ Hz. Hence, the corresponding normalized noise equivalent absorption (NNEA) coefficient for H_2S was 3.05×10^{-9} W cm^{-1} $Hz^{-1/2}$.

To evaluate the long-term stability of our system, the Allan deviation analysis was performed, by measuring and averaging the QEPAS signal for pure N_2 at 250 mbar (Fig. 8). Analysis of measurement series shows that the dominant noise in the system follows from thermal noise of the QTF (although small oscillations over $1/\sqrt{t}$ dependence can also be seen). For 60 s integration time, the sensitivity of 8 ppb was reached.

A detailed comparison of the main parameters for seven different QEPAS sensors is shown in Table 1.

Table 1 Comparison of QEPAS sensor parameters for detecting trace levels of H_2S

	Kosterev et al. [31]	Viciani et al. [26]	Siciliani de Cumis et al. [27]	Spagnolo et al. [30]	Wu et al. [40]	This paper
Laser source	DFB DL	Nanoplus DFB DL	Daylight solutions MHF EC-QCL	THz QCL	FITEL, DFB DL + EDFA[a]	Daylight solutions, MHF EC-QCL
Operating region	Near-IR	Near-IR	Mid-IR	THz	Near-IR	Mid-IR
ADM configuration	On-beam	On-beam	On-beam	Bare QTF	Off-beam	Off-beam
Wavelength (μm)	1.582	2.64	7.89	103	1.582	8.01
Laser beam power (mW)	38.3	3	45	0.24	1402	118
Line strength (10^{-22} cm/mol)	1.1	16.7	15.1	1.13	1.1	7.77
NNEA (10^{-9} cm^{-1} $W/\sqrt{Hz}$)	–	2.4	21	0.44	9.8	3.05
Sensitivity [ppb] @ integration time	10100 @ 1s	4000 @ 1s 500 @ 60s	1300 @ 1s 330 @ 30s	1300 @ 30s	734 @ 1s 142 @ 67s	492 @ 1s 8 @ 60s

[a] Erbium-Doped Fiber Amplifier (Connect Laser Technology Ltd.)

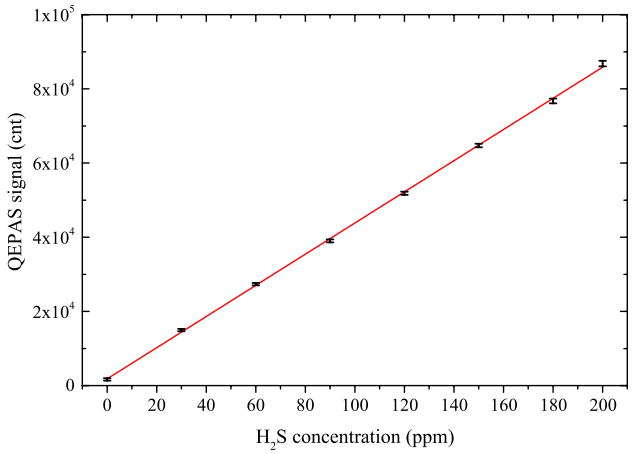

Fig. 7 QEPAS signal (2*f* detection) as a function of H_2S concentration (*red line*—linear fit)

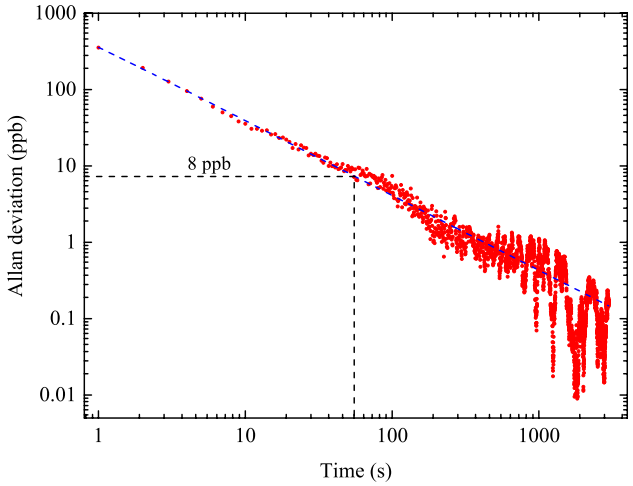

Fig. 8 Allan deviation analysis (in ppb) of the QEPAS signal with 1-s integration time, the signal was measured at 1234.26 cm^{-1} as a function of the data averaging time, for pure N_2 at 250 mbar

4 Conclusions

The results reported in this paper show that a widely tunable off-beam QEPAS spectrometer based on the MHF CW EC-QCL operating in the range of 1310–1210 cm^{-1} offered sensitive detection of H_2S, sufficient for a number of practical applications ranging from process control to environmental sensing. The CW MHF EC-QCL was tested and the obtained results were analyzed. The QEPAS system for H_2S sensing was calibrated for dry H_2S:N_2 mixture. Background free spectral scans for different H_2S concentrations were recorded to verify the sensor linearity. For the H_2S line centered at 1234.58 cm^{-1}, a minimum detection limit of 492 ppbv was achieved, which corresponded to the NNEA coefficient of 3.05×10^{-9} W cm^{-1} $Hz^{-1/2}$.

Acknowledgements MH and AD acknowledge financial support by the Research Project of Poznan University of Technology 06/62/DSPB/2171. HM and BL acknowledge financial support provided by the Austrian research funding association FFG under the scope of the COMET program within the research network imPACts (contract #843546).

References

1. A. Stanislaus, A. Marafi, M.S. Rana, Catal. Today **153**, 1 (2010)
2. European Agency for Safety and Health at Work, Occupational Exposure Limits OSHA [Internet]. Available from: https://osha.europa.eu/en/topics/ds/oel
3. S.K. Pandey, K.H. Kim, K.T. Tang, TrAC-Trends Anal. Chem. **32**, 87 (2012)
4. J.F.D.S. Petruci, P.R. Fortes, V. Kokoric, A. Wilk, I.M. Raimundo, A.A. Cardoso, B. Mizaikoff, Analyst **139**, 198 (2014)
5. H. Moser, B. Lendl, Appl. Phys. B **122**, 83 (2016)
6. A.A. Kosterev, G. Wysocki, Y. Bakhirkin, S. So, R. Lewicki, M. Fraser, F. Tittel, R.F. Curl, Appl. Phys. B **90**, 165 (2007)
7. R.F. Curl, F. Capasso, C. Gmachl, A.A. Kosterev, B. McManus, R. Lewicki, M. Pusharsky, G. Wysocki, F.K. Tittel, Chem. Phys. Lett. **487**, 1 (2010)
8. G. Hancock, G. Ritchie, J.-P. van Helden, R. Walker, D. Weidmann, Opt. Eng. **49**, 111121 (2010)
9. J.B. McManus, M.S. Zahniser, D.D. Nelson, J.H. Shorter, S. Herndon, E. Wood, R. Wehr, Opt. Eng. **49**, 111124 (2010)
10. J. Faist, C. Gmachl, F. Capasso, C. Sirtori, D.L. Sivco, J.N. Baillargeon, A.Y. Cho, Appl. Phys. Lett. **70**, 2670 (1997)
11. G.P. Luo, C. Peng, H.Q. Le, S.S. Pei, W.-Y. Hwang, B. Ishaug, J. Um, J.N. Baillargeon, C.-H. Lin, Appl. Phys. Lett. **78**, 2834 (2001)
12. J.B. McManus, D.D. Nelson, S.C. Herndon, J.H. Shorter, M.S. Zahniser, S. Blaser, L. Hvozdara, A. Muller, M. Giovannini, J. Faist, Appl. Phys. B **85**, 235 (2006)
13. H. Moser, A. Genner, J. Ofner, C. Schwarzer, G. Strasser, B. Lendl, Opt. Express **24**, 6572 (2016)
14. D.S. Bomse, A.C. Stanton, J.A. Silver, Appl. Opt. **31**, 718 (1992)
15. P. Kluczynski, J. Gustafsson, Å.M. Lindberg, O. Axner, Spectrochim. Acta Part B. At. Spectrosc. **56**, 1277 (2001)
16. H. Moser, W. Plz, J. P. Waclawek, J. Ofner, B. Lendl, Anal. Bioanal. Chem. **409**, 729 (2016)
17. A. Miklos, P. Hess, Z. Bozki, Rev. Sci. Instrum. **72**, 1937 (2001)
18. A.A. Kosterev, Y.A. Bakhirkin, R.F. Curl, F.K. Tittel, Opt. Lett. **27**, 1902 (2002)
19. J.-M. Friedt, E. Carry, Am. J. Phys. **75**, 415 (2007)
20. A. A. Kosterev, F. K. Tittel, D. V. Serebryakov, A. L. Malinovsky, I. V. Morozov, Rev. Sci. Instrum. **76**, 043105:1 (2005)
21. L. Dong, A.A. Kosterev, D. Thomazy, F.K. Tittel, Appl. Phys. B **100**, 627 (2010)
22. K. Liu, X. Guo, H. Yi, W. Chen, W. Zhang, X. Gao, Opt. Lett. **34**, 1594 (2009)
23. H. Yi, W. Chen, X. Guo, S. Sun, K. Liu, T. Tan, W. Zhang, X. Gao, Appl. Phys. B **108**, 361 (2012)
24. M. Lassen, L. Lamard, Y. Feng, A. Peremans, J.C. Petersen, Opt. Lett. **41**, 4118 (2016)

25. M. Jahjah, W. Jiang, N.P. Sanchez, W. Ren, P. Patimisco, V. Spagnolo, S.C. Herndon, R.J. Griffin, F.K. Tittel, Opt. Lett. **39**, 957 (2014)
26. S. Viciani, M. Siciliani de Cumis, S. Borri, P. Patimisco, A. Sampaolo, G. Scamarcio, P. De Natale, F. DAmato, and V. Spagnolo. Appl. Phys. B **119**, 21 (2015)
27. M. Siciliani de Cumis, S. Viciani, S. Borri, P. Patimisco, A. Sampaolo, G. Scamarcio, P. De Natale, F. DAmato, and V. Spagnolo. Opt. Express **22**, 28222 (2014)
28. S. Borri, P. Patimisco, A. Sampaolo, H.E. Beere, D.A. Ritchie, M.S. Vitiello, G. Scamarcio, V. Spagnolo, Appl. Phys. Lett. **103**, 21105 (2013)
29. P. Patimisco, S. Borri, A. Sampaolo, H.E. Beere, D.A. Ritchie, M.S. Vitiello, G. Scamarcio, V. Spagnolo, Analyst **139**, 2079 (2014)
30. V. Spagnolo, P. Patimisco, R. Pennetta, A. Sampaolo, G. Scamarcio, M.S. Vitiello, F.K. Tittel, Opt. Express **23**, 7574 (2015)
31. A.A. Kosterev, L. Dong, D. Thomazy, F.K. Tittel, S. Overby, Appl. Phys. B **101**, 649 (2010)
32. H. Wu, A. Sampaolo, L. Dong, P. Patimisco, X. Liu, H. Zheng, X. Yin, W. Ma, L. Zhang, W. Yin, V. Spagnolo, S. Jia, F.K. Tittel, Appl. Phys. Lett. **107**, 2 (2015)
33. W. Uhmann, A. Becker, C. Taran, F. Siebert, Appl. Spectrosc. **45**, 390 (1991)
34. T.J. Johnson, A. Simon, J.M. Weil, G.W. Harris, Appl. Spectrosc. **47**, 1376 (1993)
35. L.S. Rothman, I.E. Gordon, Y. Babikov, A. Barbe, D. Chris, Benner, P. F. Bernath, M. Birk, L. Bizzocchi, V. Boudon, L. R. Brown, A. Campargue, K. Chance, E. A. Cohen, L. H. Coudert, V. M. Devi, B. J. Drouin, A. Fayt, J. M. Flaud, R. R. Gamache, J. J. Harrison, J. M. Hartmann, C. Hill, J. T. Hodges, D. Jacquemart, A. Jolly, J. Lamouroux, R. J. Le Roy, G. Li, D. A. Long, O. M. Lyulin, C. J. Mackie, S. T. Massie, S. Mikhailenko, H. S. P. Mller, O. V. Naumenko, A. V. Nikitin, J. Orphal, V. Perevalov, A. Perrin, E. R. Polovtseva, C. Richard, M. A. H. Smith, E. Starikova, K. Sung, S. Tashkun, J. Tennyson, G. C. Toon, V. G. Tyuterev, G. Wagner, J. Quant. Spectrosc. Radiat. Transf. **130**, 4 (2013)
36. H.-J. Bauer, A.C.C. Paphitis, R. Schotter, Physica **47**, 109 (1970)
37. H. Yi, W. Chen, S. Sun, K. Liu, T. Tan, X. Gao, Opt. Express **20**, 9187 (2012)
38. J.P. Waclawek, R. Lewicki, H. Moser, M. Brandstetter, F.K. Tittel, B. Lendl, Appl. Phys. B **117**, 113 (2014)
39. H. Wu, L. Dong, W. Ren, W. Yin, W. Ma, L. Zhang, S. Jia, F.K. Tittel, Sens. Actuator B **206**, 364 (2014)
40. H. Wu, L. Dong, H. Zheng, X. Liu, X. Yin, W. Ma, L. Zhang, W. Yin, S. Jia, F.K. Tittel, Sens. Actuator B **221**, 666 (2015)